Three-dimensional hexapole focusing of pulsed molecular beam for state selection*

Yi Ke(柯毅), Xiao-Bing Deng(邓小兵), and Zhong-Kun Hu(胡忠坤)†

Key Laboratory of Fundamental Physical Quantities Measurements, Ministry of Education, School of Physics, Huazhong University of Science and Technology, Wuhan 430074, *China*

(Received 22 February 2017; revised manuscript received 26 April 2017; published online 20 June 2017)

We theoretically investigate three-dimensional (3D) focusing of pulsed molecular beam using a series of hexapoles with different orientations. Transversely oriented hexapoles provide both the transverse and longitudinal focusing force and a longitudinally oriented one provides only the transverse force. The hexapole focusing position are designed to realize the simultaneous focusing in three directions. The additional longitudinal focusing compared with the conventional hexapole can suppress the effect of chromatic aberration induced by the molecular longitudinal velocity spread, thus improving the state-selection purity as well as the beam density. Performance comparison of state selection between this 3D focusing hexapole and a conventional one is made using numerical trajectory simulations, choosing CHF_3 molecules as a tester. It is confirmed that our proposal can improve the state-selection purity from 68.2% to 96.1% and the beam density by a factor of 2.3.

Keywords: hexapole, focusing, state selection, chromatic aberration

PACS: 37.20.+j **DOI:** 10.1088/1674-1056/26/8/083701

1. Introduction

Since the technique of electrostatic hexapole was introduced half a century ago,[1–4] it is demonstrated to be a quite powerful tool to focus molecular beams and realize the state selection.[5,6] The state-selected molecular beams are ideal starting points for experiments of photodissociation,[7–9] photoionization,[10,11] surface scattering,[12–14] inelastic or elastic scattering,[15–18] and further laser-induced alignment and orientation,[19–21] etc. In these experiments, preparing initial molecular beam with high state purity and beam density is usually a key point. For example, in scattering experiments, preparing molecules in a pure quantum state is necessary to measure the state-to-state cross sections. In reactive scattering experiments, particular those with small cross sections, high beam density would be crucial.

The molecules with first-order Stark effect in the inhomogeneous electric field inside the hexapole will experience a transverse harmonic force towards to the hexapole axis while there is no longitudinal force. The molecular trajectories of a particular quantum state will be focused to the exit aperture to realize the state selection. This process is analogous to the optical imaging. The typical 10%∼20% longitudinal velocity spread of the molecular beam will lead to the phenomenon of chromatic aberration, i.e., molecules with different longitudinal velocities will be focused at different positions. The chromatic aberration effect will broaden the focusing curve and reduce the state purity. Meanwhile, since the molecules fly freely in the longitudinal direction, the molecular packet will spread out, thus reducing the beam density.

Previously we have proposed a useful low chromatic aberration hexapole scheme to suppress the chromatic aberration effect.[22] By switching off the hexapole voltage rapidly at an appropriate time, the focusing positions of all molecules are very close. However, in that scheme, the molecules fly freely in the longitudinal direction and the focusing moments are not the same. Thus the beam density is low at the focusing point. In this work, we present a three-dimensional (3D) focusing hexapole scheme to further focus the molecular beam in the longitudinal direction compared with the conventional hexapole. The experimental device consists of a series of transversely oriented hexapoles and a longitudinally oriented one. The longitudinal focusing force is provided by the transversely oriented hexapoles and the longitudinally oriented hexapole is used to adjust the transverse focusing time to realize the simultaneous focusing in three directions, i.e., two transverse directions and one longitudinal direction. The hexapole voltages are all operated in a pulse mode so that the molecules experience a force during an equal time and the focusing times are independent of the longitudinal velocity. This scheme can improve the state-selection purity as well as the beam density at the focusing point. This paper is a theoretical paper without experiments.

Longitudinal focusing of a pulsed molecular beam after Stark deceleration has been experimentally demonstrated using a buncher whose operation principle is equivalent to that of the Stark decelerator operated at a phase angle of 0°.[23] Very recently, quadrupole lenses combined with bunching elements

*Project supported by the National Natural Science Foundation of China (Grant Nos. 11504118, 11574099, and 11474115).

†Corresponding author. E-mail: zkhu@hust.edu.cn

© 2017 Chinese Physical Society and IOP Publishing Ltd

are used to focus decelerated and cooled molecules at the detection region in a molecular fountain.[24] Here we design the hexapole voltages and pulse sequence to realize a simultaneous 3D spatial focusing of a pulsed molecular beam.

The layout of this paper is as follows. First, we present the details of the 3D hexapole focusing scheme and the principle of parameter design. Then, performance of this 3D focusing hexapole is compared with that of a conventional hexapole using numerical trajectory simulations, choosing CHF_3 molecules as a tester. Finally, the conclusions are presented.

2. Scheme of 3D focusing hexapole

The hexapole consists of an arrangement of six rod electrodes, which are alternately charged to voltage $+V_0$ and $-V_0$. This configuration produces an inhomogeneous electric field inside the hexapole and the strength E depends on the distance r from the hexapole axis. The electric field strength can be expressed to a good approximation as[1,25]

$$E = \left(\frac{3V_0}{r_0^3}\right) r^2, \tag{1}$$

where r_0 is the hexapole radius. In this inhomogeneous field, the radial force felt by a molecule with a linear Stark shift in a low-field-seeking state is a harmonic one towards to the center axis of the hexapole which can be written as

$$F_r = -m\omega^2 r, \tag{2}$$

where m is the mass of the molecule. The angular frequency ω depends on the molecular species and the quantum state. For a symmetric top molecule,

$$\omega = \sqrt{\frac{-6\mu KMV_0}{mJ(J+1)r_0^3}}, \tag{3}$$

where J is the rotational quantum number, and K and M are the quantum numbers describing the projections of molecular angular momentum on the molecule-fixed axis and the spaced-fixed axis, respectively. μ is the permanent electric dipole moment of the molecule.

The focusing equation of a conventional hexapole can be found in Ref. [26]. In our previous work, we also derived it by tracing the deformations of molecular phase-space distribution in free flights and the harmonic potential. The result is given by[22]

$$L_3 = \frac{1}{k}\cot\left[kL_2 - \arctan\left(\frac{1}{kL_1}\right)\right], \tag{4}$$

where $k \equiv \omega/v_z$ is the lens constant[27] with v_z being the molecular longitudinal velocity. L_1 and L_3 are the lengths of the free-flight regions at the beginning and end of the focusing process, respectively. L_2 is the length of the hexapole focusing region. We use T_1, T_2, and T_3 to denote the molecular flight time in the L_1, L_2, and L_3 regions, respectively. Equation (4) can be rewritten as

$$T_3 = \frac{1}{\omega}\cot\left[\omega T_2 - \arctan\left(\frac{1}{\omega T_1}\right)\right]. \tag{5}$$

The conventional hexapole is oriented along the longitudinal direction (molecular beam axis direction). Molecules in the hexapole are focused in two transverse directions and free in the longitudinal direction. The molecular longitudinal velocity spread will induce a spread of the molecular focusing positions, thus reducing the state-selection purity. Also the spread of the molecular packet will reduce the beam density. In order to reduce the longitudinal spread of the focusing positions and the packet, molecules should be longitudinally focused. The longitudinal focusing force can also be provided by the hexapole by means of orienting the hexapole transversely. The focusing region length of a transversely oriented hexapole is limited by the diameter of the hexapole, which is much shorter than the focusing region length of a conventional hexapole. The short focusing region length requires high hexapole voltage and thus strong electric field strength to realize the molecular longitudinal focusing. In order to realize the molecular longitudinal focusing under an experimentally available hexapole voltage and electric field strength, more than one transversely oriented hexapoles are needed.

The proposed experimental scheme is shown in Fig. 1. The molecules coming from a pulsed valve first fly through a series of transversely oriented (x- or y-oriented) hexapoles. In the diagram, six transversely oriented hexapoles are drawn. However, the number of the transversely oriented hexapoles is not necessarily six. A transversely oriented hexapole can focus molecules in the z direction (molecular beam axis direction) and either the x or y direction. The y- and x-oriented hexapoles are arranged alternately to focus molecules in the x and y directions in turn while the z direction are always be focused. Through the transversely oriented hexapoles, molecules are less focused in the x and y directions than in the z direction. Downstream the transversely oriented hexapoles, a longitudinally oriented hexapole is placed to further focus molecules in the x and y directions and realize the simultaneous focusing in three directions. The hexapole voltages are all operated in a pulse mode so that the molecules experience a force during an equal time and the focusing times are independent of the longitudinal velocity. When the main part of the molecular packet is inside one hexpole, the voltages of the other hexapoles are switched off.

The molecular focusing process using a harmonic potential well can be described by the transformation of the molecular phase-space distribution. The description of the transverse focusing process can be found in Ref. [22] and can be extended

to the longitudinal focusing case. In our scheme, the focusing time of each direction is calculated based on the focusing time equation (5). Like the lens focusing formula in geometric optics, equation (5) can be applied to the focusing process using a series of hexapole lens. Subtracting the T_3 time of the former hexapole focusing process from the time interval between two hexapole voltage pulses gives the T_1 time of the latter hexapole focusing process.

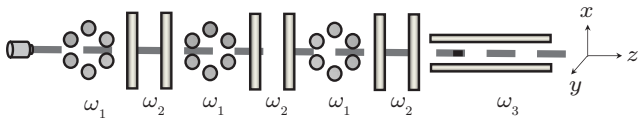


Fig. 1. Schematic diagram of the 3D hexapole focusing experimental device consisting of a series of transversely oriented hexapoles and a longitudinally oriented one. ω_1, ω_2 and ω_3 denote the different angular frequencies of the molecular harmonic motions in the hexapoles.

The focusing time of molecules in each direction depends on the molecular Stark effect and forward velocity, the geometry of the hexapoles, the switching moments of the voltage pulses that are applied to the hexapoles, and the magnitude of the hexapole voltages. In the parameter design of the device, the molecular properties and the geometry of the hexapoles are first set. We define the molecule in the target state to be selected out which has no transverse velocity and the longitudinal center velocity of the molecular beam as the synchronous molecule. We determine the switch-on and switch-off moments of each hexapole when the synchronous molecule arrives at a certain position inside the hexapole. After that, the focusing times only depend on the hexapole voltages.

For simplicity, the voltages of the hexapoles with the same orientation can be set to be the same. A hexapole voltage corresponds to an angular frequency of the molecular harmonic motions inside the hexapole. We use ω_1, ω_2, and ω_3 to denote the angular frequencies in the y-, x-, and z-oriented hexapoles, respectively. Firstly, we set the value of ω_1. After that, the value of ω_2 is found to let the molecular focusing times of the x and y directions to be the same after flying through the transversely oriented hexapoles. The molecular longitudinal focusing time is determined after the determination of the ω_1 and ω_2 values. The focusing effects in the x and y directions of the last z-oriented hexapole are identical, so the focusing times of the x and y directions will still be equal after molecules fly through the last hexapole. We can adjust the value of ω_3 to let the focusing times in the x and y directions to be identical with that in the z direction.

3. Performance comparison between 3D focusing hexapole and conventional one

To compare the performance of the 3D focusing hexapole with that of the conventional hexapole in state selection, the method of numerical trajectory simulations is used. The oblate symmetric top molecule CHF_3 is used in the simulations, as in our previous work.[22]

The electric dipole moment μ of the CHF_3 molecule is 1.65 Debye and the rotational constants are $A = B =$ 10.35 GHz and $C = 5.67$ GHz.[28] In the simulations, the average forward velocity of the pulsed CHF_3 molecular beam is set to be 300 m/s, which can be realized via a low-temperature pulsed valve[23,29,30] This relatively low forward velocity helps to reduce the voltage requirements of the transversely oriented hexapoles since molecules spend more time in the focusing region. The velocity distributions of the initial molecular beam in all directions are independent Gaussian ones. The full width at half maximum (FWHM) in the transverse direction is 5 m/s and 30 m/s in the longitudinal direction. The initial transverse spatial distribution at the valve is also assumed to be Gaussian with an FWHM of 0.1 mm. The molecular pulse also has an initial duration at the valve. We assume the pulse has a Gaussian temporal function with a duration of 10 μs, which can be realized by recently reported short-pulse vales.[31–33] The rotational temperature of the molecular beam is set to be 2 K. The equal population is assumed for different M states while the quantum numbers J and K are the same. In the simulations, we only consider rotational states with a first-order Stark effect. At the rotational temperature of 2 K, the states with rotational quantum number $J = 3$ and $K = 3$ or -3 are most populated among the states being considered. Among these states, we choose low-field-seeking $|J = 3, K = 3, M = -3\rangle$ and $|J = 3, K = -3, M = 3\rangle$ states as the target states to be selected out which has a population of 3.01%. We designate both the two states as $|333\rangle$ for simplicity.

The parameters of the 3D focusing hexapole are designed as follows. The number of the transversely oriented hexapoles is set to be six. The distance between the nozzle and the center axis of the first transversely oriented hexapole is set to be 17 cm. The radii of the transversely oriented hexapoles are all set to be 10 mm. The radius of the cylindrical rods of the hexapole is set to be 0.565 of the hexapole radius, as recommended by Anderson.[25] The distance between the center axes of nearby transversely oriented hexapole is set to be twice the hexapole diameter, i.e., 40 mm. The flight region of the synchronous molecule when the voltage of the transversely oriented hexapole is on is set to be symmetrical about the hexapole axis with a length of hexapole radius, i.e., 10 mm. The value of ω_1 is set to be 3400 rad/s, and correspondingly the value of ω_2 is determined to be 3103 rad/s. These values correspond to hexapole voltages of 54.2 kV and 45.1 kV and maximum electric field strengths of 162 kV/cm and 135 kV/cm, respectively. The radius of the last longitudinally oriented hexapole is set to be 4 mm. The voltage switch-on moment is set to be 233 μs after the switch-off moment of the last transversely oriented hexapole, and the voltage pulse

duration is set to be 333 μs. The exit aperture is placed in the focusing position of the synchronous molecule, which is calculated to be 809 mm downstream the nozzle. The flight time of the synchronous molecule from the nozzle to the aperture is 2.70 ms. The parameters of the conventional hexapole for comparison are set as follows. The radius of the conventional hexapole is set to be 4 mm and the aperture position is set to be the same as the 3D focusing hexapole. The ratio of L_1, L_2, and L_3 is set to be 0.15:0.7:0.15. The radius and position parameters of the skimmer, beamstop and aperture are given in Table 1. The origin of the z axis coincides with the position of the pulsed nozzle.

Table 1. List of parameters of the 3D focusing hexapole and the conventional hexapole.

Component	Radius/mm	z-axis position/cm	
		3D focusing	Conventional
Skimmer	0.5	3.0	3.0
Beamstop	1.0	45.7	40.5
Aperture	0.1	80.9	80.9

In the simulations, the initial CHF_3 molecular beam contains 1.00×10^8 molecules. Among these, there are 3.01×10^6 molecules in the target $|333\rangle$ state. We only consider the states which are low-field seekers and have an initial population more than 0.01 percent of the target state. The time step used in the numerical integration of molecular trajectories is about 0.2 μs. The ideal electric field distribution inside the hexapole is used in the calculation. We assume molecules which are blocked by the skimmer, the beamstop, or the hexapoles disappear. A molecule is considered to be transmitted through the hexapole if its radial displacement at the exit is smaller than the radius of the exit aperture.

The parameters of the 3D focusing hexapole designed above is based on Eq. (5), which is derived in the ideal case, i.e., a point molecular source and linear Stark effect. To confirm that the designed parameters are correct, we first use a point molecular source in the simulation. The initial width of transverse distribution and the pulse duration are all set to be zero. Only the first-order Stark effect is taken into consideration. In this situation, the target molecules are expected to be focused into a point. The calculated phase-space distributions of the molecules in the $|333\rangle$ state at the moment that the synchronous molecule is arriving at the aperture are shown in Fig. 2. In the figure, panels (a), (b), and (c) are the phase-space distributions projected onto the x–v_x, y–v_y, and z–v_z planes, respectively. In depicting the distributions, the $|333\rangle$ state molecules have an initial number of 1.5×10^4. For optimum performance of the 3D focusing, all the molecules should be inside the hexapole when the pulsed voltage is applied. However, there are many molecules outside the transversely oriented hexapole when the pulsed voltage is applied due to the longitudinal dispersion. These molecules will not be fully focused. In Fig. 2, the molecules which have fully experienced all the focusing processes of the hexapoles are distributed on a vertical line, indicating a perfect spatial focusing into a point. The molecules that are not fully focused are distributed over a spatial region. The molecules that have a large difference in longitudinal velocity between the synchronous molecule will not experience all the first six focusing processes, owing to the large longitudinal dispersion. The phase-space distributions of these molecules projected onto the x–v_x or y–v_y plane will be a straight line, forming the boundary line in Figs. 2(a) or 2(b).

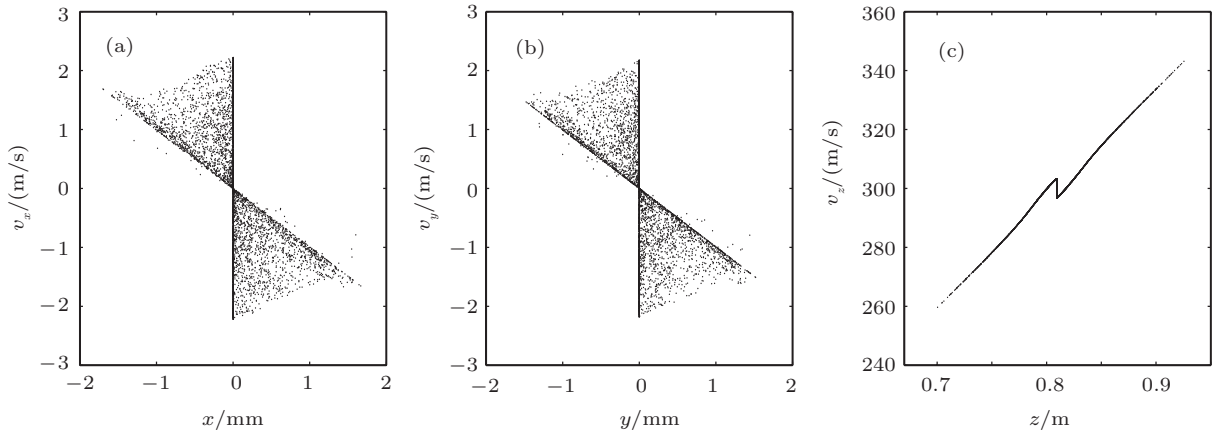


Fig. 2. The calculated phase-space distributions of the molecules in the $|333\rangle$ state at the moment that the synchronous molecule is arriving at the aperture for the 3D focusing hexapole.

Due to the high electric field strength in the transversely oriented hexapoles, the nonlinear Stark effect should not be neglected. The first-order Stark interaction energy given by the first-order perturbation calculation is the diagonal element of the interaction Hamiltonian[34]

$$W^{(1)}_{\text{Stark}} = \langle JKM|H_{\text{i}}|JKM\rangle = -\frac{KM}{J(J+1)}\mu E, \qquad (6)$$

where H_{i} is the Hamiltonian of the interaction of the electric field E with the electric dipole moment μ. The second-order

Stark effect is given by the second-order perturbation as[34]

$$W_{\text{Stark}}^{(2)} = \frac{\mu^2 E^2}{2hB}\left\{\frac{(J^2-K^2)(J^2-M^2)}{J^3(2J-1)(2J+1)} - \frac{[(J+1)^2-K^2][(J+1)^2-M^2]}{(J+1)^3(2J+1)(2J+3)}\right\}, \quad (7)$$

with h the Planck constant. The exact Stark energy is determined by diagonalizing the total Hamiltonian of the field free molecule and the interaction. The total Hamiltonian matrix is tridiagonal. The nondiagonal matrix elements of the interaction Hamiltonian are[34]

$$\langle J+1,K,M|H_{\text{i}}|J,K,M\rangle = \frac{[(J+1)^2-K^2]^{1/2}[(J+1)^2-M^2]^{1/2}}{(J+1)[(2J+1)(2J+3)]^{1/2}}, \quad (8)$$

$$\langle J-1,K,M|H_{\text{i}}|J,K,M\rangle = \frac{(J^2-K^2)^{1/2}(J^2-M^2)^{1/2}}{J[(2J-1)(2J+1)]^{1/2}}. \quad (9)$$

We calculate the Stark effect to the first order, second order and using the exact Stark interactions. Figure 3(a) is the calculated Stark energies and figure 3(b) is the effective force constants, i.e., $(1/\mu)(\mathrm{d}W_{\text{Stark}}/\mathrm{d}E)$,[25] which is proportional to the the force that the molecules experience. The maximum electric field strength in the 3D focusing hexapole is about 162 kV/cm. In this strength even the inclusion of the second-order Stark effect cannot exactly describe the Stark effect. Therefore we use the exact Stark interactions in the simulations below. Due to the nonlinear Stark effect, the focusing in each direction will not be perfect and the focusing times in three directions will not be simultaneous. Since the force is smaller in the exact Stark case, as can be seen from Fig. 3(b), the molecular focusing positions will be further downstream. In the simulations using the exact Stark interactions, the position of the exit aperture is moved downstream in order to be closer to the focusing positions. By comparing the state-selection results with different position shifts of the aperture, we choose a position shift of 12 mm which corresponds to a relatively large final molecular number, beam density and state-selection purity.

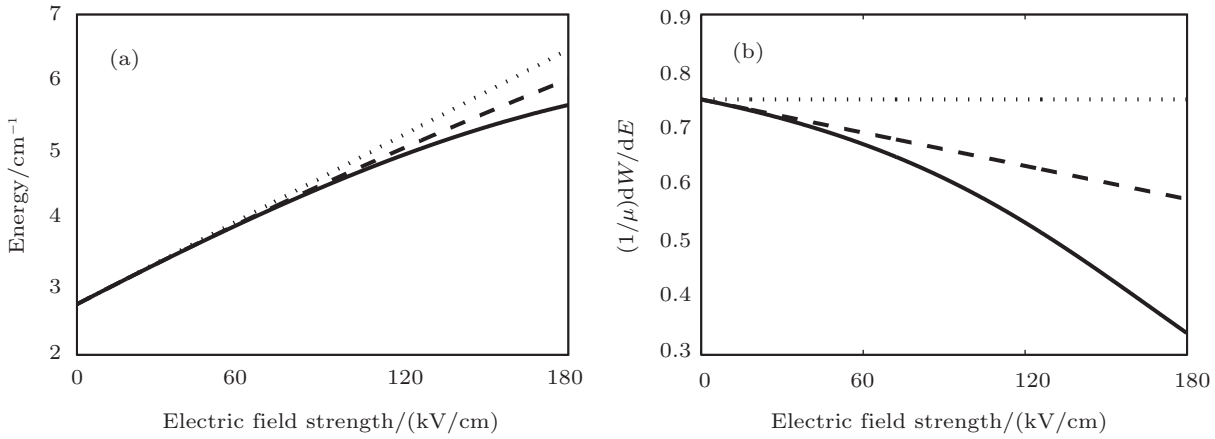


Fig. 3. The calculated Stark energies (a) and effective force constants (b) of the CHF_3 molecule in the $|333\rangle$ state. The dotted, dashed and solid lines correspond to the calculation to the first-order, second-order Stark effect and using the exact Stark interactions, respectively.

The simulation results are given in Table 2. The 10 most populations of rotational state in the state-selected CHF_3 beam are listed along with the corresponding initial populations. The results of the 3D focusing hexapole are compared with the conventional one. The final population in the target $|333\rangle$ state is 96.1% for the 3D focusing hexapole while 68.2% for the conventional one, improved by a factor of 1.4. The final molecular number in the $|333\rangle$ state of the 3D focusing hexapole is 3.93×10^5, slightly less than that of the conventional hexapole, which is 5.21×10^5. This is because in the 3D focusing hexapole, there are many molecules not fully focused. These molecules will not successfully fly through the exit aperture.

Table 2. Initial and final populations (in %) of the state-selected CHF_3 beam through a conventional and a 3D focusing hexapole. The 10 most final populations and the corresponding initial populations are listed. The exact Stark interactions are used in the simulations.

Conventional hexapole			3D focusing hexapole		
State	Initial	Final	State	Initial	Final
$\|333\rangle$	3.013	68.2	$\|333\rangle$	3.013	96.1
$\|222\rangle$	2.651	22.7	$\|444\rangle$	0.315	2.6
$\|444\rangle$	0.315	5.6	$\|665\rangle$	0.036	0.5
$\|555\rangle$	0.072	0.8	$\|555\rangle$	0.072	0.5
$\|665\rangle$	0.036	0.7	$\|666\rangle$	0.036	0.2
$\|554\rangle$	0.072	0.6	$\|776\rangle$	0.002	0.1
$\|434\rangle$	0.413	0.4	$\|656\rangle$	0.004	0.0
$\|443\rangle$	0.315	0.3	$\|767\rangle$	0.001	0.0
$\|666\rangle$	0.036	0.3	$\|777\rangle$	0.002	0.0
$\|545\rangle$	0.026	0.2	$\|222\rangle$	2.651	0.0

To assess the ability of the 3D focusing hexapole to increase the beam density on the focusing point, we calculate the molecular number in the $|333\rangle$ state around the focusing point within the range of 0.1 mm, which is proportional to the beam density, for two types of hexapole. The results are shown in Fig. 4. The peak number corresponding to the focusing moment is 4084 for the conventional hexapole and 9588 for the 3D focusing one, indicating a 2.3-fold increase in the beam density via the 3D focusing hexapole. The increase of the beam density is not very high due to the imperfect molecular source. The initial transverse spatial distribution and the pulse duration of the source hinder the perfect focusing to a point.

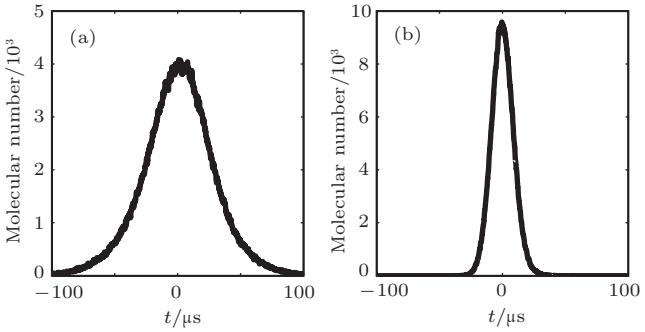


Fig. 4. The calculated density of the molecules in the the $|333\rangle$ state at the focusing point, i.e., the aperture position on the z axis, as a function of time (at $t = 0$ μs the synchronous molecule is arriving at the aperture) for two types of hexapole. Panel (a) corresponds to the case of the conventional hexpole and panel (b) the 3D focusing one.

4. Conclusions

In summary, we have presented a proposal to improve both the purity and the density of the state-selected molecular beam by using a combination of longitudinal and transverse harmonic potential wells provided by a series of transversely oriented hexapoles and a longitudinal oriented one. Performance comparison between this proposed 3D focusing hexapole and a conventional one is made using numerical trajectory simulations. In the simulations, the ideal electric field distribution inside the hexapole is used and the exact Stark energy of the CHF_3 molecule is taken into consideration. Electric field deviations from the ideal hexapole field is neglected. It is confirmed that our proposal can improve the state purity from 68.2% to 96.1% and the beam density by a factor of 2.3. For more complex polar molecules, the improvements of the purity and density of the state-selected beam of our scheme need to be further evaluated. We demonstrate theoretically the improvements of the purity and density of the state-selected beam, and the molecule loss due to collisions to the hexapole components is considered. In a realistic experiment, the extension of the molecular trajectories may induce other loss mechanisms of molecular number that have not been considered. Our proposed hexapole has promising prospects in some molecular beam experiments, e.g., molecular scattering experiments in which high state purity and beam density are desirable. The improvement of the molecular beam density is limited by the imperfect molecular source. It looks forward to the technological development of the molecular source with a narrower transverse distribution and a shorter duration.

References

[1] Kramer K H and Bernstein R B 1965 *J. Chem. Phys.* **42** 767
[2] Brooks P R and Jones E M 1966 *J. Chem. Phys.* **45** 3449
[3] Beuhler Jr R J, Bernstein R B and Kramer K H 1966 *J. Am. Chem. Soc.* **88** 5331
[4] Brooks P R, Jones E M and Smith K 1969 *J. Chem. Phys.* **51** 3073
[5] Liu F C, Jin M X, Gao X and Ding D J 2006 *Chin. Phys. Lett.* **23** 344
[6] Liu F C, Jin M X and Ding D J 2006 *Chin. Phys. Lett.* **23** 1165
[7] Gandhi S R, Curtiss T J and Bernstein R B 1987 *Phys. Rev. Lett.* **59** 2951
[8] Che D C, Hashinokuchi M, Shimizu Y, Ohoyama H and Kasai T 2001 *Phys. Chem. Chem. Phys.* **3** 4979
[9] Rakitzis T P, van den Brom A J and Janssen M H M 2004 *Science* **303** 1852
[10] Kaesdorf S, Schönhense G and Heinzmann U 1985 *Phys. Rev. Lett.* **54** 885
[11] Gijsbertsen A, Siu W, Kling M F, Johnsson P, Jansen P, Stolte S and Vrakking M J J 2007 *Phys. Rev. Lett.* **99** 213003
[12] Kuipers E W, Tenner M G, Kleyn A W and Stolte S 1989 *Phys. Rev. Lett.* **62** 2152
[13] Sitz G O 2002 *Rep. Prog. Phys.* **65** 1165
[14] Berenbak B, Riedmüller B, Stolte S and Kleyn A W 2004 *Chem. Phys.* **301** 309
[15] Brooks P R 1976 *Science* **193** 11
[16] van Beek M C, Berden G, Bethlem H L and ter Meulen J J 2001 *Phys. Rev. Lett.* **86** 4001
[17] Kirste M, Wang X, Schewe H C, Meijer G, Liu K, van der Avoird A, Janssen L M C, Gubbels K B, Groenenboom G C and van de Meerakker S Y T 2012 *Science* **338** 1060
[18] Nichols B, Chadwick H, Gordon S, Eyles C, Hornung B, Brouard M, Alexander M, Aoiz F, Gijsbertsen A and Stolte S 2015 *Chem. Sci.* **6** 2202
[19] Sakai H, Minemoto S, Nanjo H, Tanji H and Suzuki T 2003 *Phys. Rev. Lett.* **90** 083001
[20] Ghafur O, Rouzée A, Gijsbertsen A, Siu W K, Stolte S and Vrakking M J J 2009 *Nat. Phys.* **5** 289
[21] Luo S, Zhu R, He L, Hu W, Li X, Ma P, Wang C, Liu F, Roeterdink W G, Stolte S and Ding D 2015 *Phys. Rev. A* **91** 053408
[22] Ke Y, Deng X B and Hu Z K 2016 *J. Phys. B: At. Mol. Opt. Phys.* **49** 025101
[23] Crompvoets F M H, Jongma R T, Bethlem H L, van Roij A J A and Meijer G 2002 *Phys. Rev. Lett.* **89** 093004
[24] Cheng C, van der Poel A P P, Jansen P, Quintero-Pérez M, Wall T E, Ubachs W and Bethlem H L 2016 *Phys. Rev. Lett.* **117** 253201
[25] Anderson R W 1997 *J. Phys. Chem. A* **101** 7664
[26] Stolte S, Reuss J and Schwartz H L 1972 *Physica* **57** 254
[27] Cho V A and Bernstein R B 1991 *J. Phys. Chem.* **95** 8129
[28] Meerts W L and Ozier I 1981 *J. Chem. Phys.* **75** 596
[29] Bethlem H L, van Roij A J, Jongma R T and Meijer G 2002 *Phys. Rev. Lett.* **88** 133003
[30] Jung S, Tiemann E and Lisdat C 2006 *Phys. Rev. A* **74** 040701
[31] Even U, Jortner J, Noy D, Lavie N and Cossart-Magos C 2000 *J. Chem. Phys.* **112** 8068
[32] Hillenkamp M, Keinan S and Even U 2003 *J. Chem. Phys.* **118** 8699
[33] Irimia D, Dobrikov D, Kortekaas R, Voet H, van den Ende D A, Groen W A and Janssen M H 2009 *Rev. Sci. Instrum.* **80** 113303
[34] Gordy W and Cook R L 1984 *Microwave Molecular Spectra*, 3rd edn. (New York: Wiley)